THE JOURNAL OF BIOLOGICAL CHEMISTRY
Vol. 277, No. 47, Issue of November 22, pp. 44980–44987, 2002
Printed in U.S.A.

The Structural Organization of Cationic Lipid-DNA Complexes*

Received for publication, July 31, 2002, and in revised form, September 16, 2002
Published, JBC Papers in Press, September 23, 2002, DOI 10.1074/jbc.M207758200

Christopher M. Wiethoff‡§, Michelle L. Gill‡¶, Gary S. Koe‖, Janet G. Koe‖, and C. Russell Middaugh‡

From the ‡Department of Pharmaceutical Chemistry, The University of Kansas, Lawrence, Kansas 66047 and ‖Valentis, Inc., Burlingame, California 94010

The interaction of cationic liposomes with supercoiled plasmid DNA results in a major rearrangement of each component to form compact multilamellar structures comprised of alternating layers of two-dimensional arrays of DNA sandwiched between lipid bilayers. Fluorescence resonance energy transfer was used to estimate the distance of closest approach of DNA to the lipid bilayers in these complexes. The effect of several compositional variables on this distance, including the ratio of cationic lipid to DNA, and the charge density, intrinsic curvature, and fluidity of the lipid bilayer were examined. Additionally, the effect of ionic strength was studied. For complexes prepared at or above a 3:1 charge ratio (+/−), the observed distance of closest approach was found to be in agreement with the intercalation of DNA between lipid bilayers. As the charge ratio was decreased, a monotonic increase in the distance was observed with a maximum observed at 0.5:1. Correlations between differences in the proximity of DNA to the lipid bilayer and the hydrodynamic size of the complexes were also found. A model based on these observations and previous reports suggests the formation of discrete populations of complexes below a charge ratio of 0.5:1 and above 3:1. The structure of the negatively charged complexes is consistent with DNA extending from the surface of the particles, whereas those possessing excess positive charge were multilamellar aggregates with the DNA effectively condensed between lipid bilayers. Complexes between these two states consist of weighted fractions of these two species.

The use of cationic lipids to deliver DNA into cells has received considerable attention for applications in gene therapy (1–3). Condensation of negatively charged DNA into cationic lipid-DNA complexes (CLDCs)[1] is thought to aid in the delivery of the DNA to the cell nucleus by protecting it from enzymatic degradation in extracellular compartments, facilitating binding to the negatively charged cell surface and aiding in penetration of DNA into the cytosol (4). Numerous studies have suggested that the efficiency of this delivery process is related in a still ill-defined way to a variety of physical and chemical properties of the CLDC (5–17). Most notably, the colloidal properties and composition of the CLDCs appear to have major effects on transfection efficiency both *in vitro* (5) and *in vivo* (18).

Given the lack of clear structure/function correlations, a significant effort has been put into the study of the structures that result from mixing cationic liposomes with DNA. The formation of CLDCs appears to involve initial DNA-induced aggregation of the cationic liposomes followed by vesicle rupture and fusion (6, 16, 19–22), the result of which is a fairly heterogeneous distribution of particles in terms of shape and size. Qualitatively, these particles typically appear globular in nature when cationic lipids are present in charge excess and are often observed to have tubular strands protruding from the particle surface when DNA is present in charge excess (6). On a smaller scale, highly ordered lamellar arrays composed of alternating stacks of DNA and lipid bilayers are observed in these complexes by cryoelectron microscopy (6, 8, 9, 22–24) and small angle x-ray scattering (10, 14, 15, 25). The lamellar spacing appears to be a function of the type of lipid used (14), the ratio of cationic lipid to DNA (6), and the solution conditions (14). In addition to these lamellar arrays, nonlamellar structures have been observed by cryo-EM (8, 9) and SAXS (8, 15), by changing the intrinsic curvature of the membrane or its flexibility. Although these nonlamellar structures have been proposed to facilitate more efficient delivery of DNA, presumably because of their ability to cause greater disruption of endosomal membranes (26), increased transgene expression is not always observed for these systems (6, 27, 28).

Although cryo-EM and SAXS can provide significant detail about the structure of CLDCs, the conditions for obtaining measurements using these techniques are often considerably different from those used for transfection. For example, in the case of cryo-EM, the complexes are flash frozen. Although studies using SAXS have be conducted using concentrations of lipid and DNA closer to those used for transfection by employing high energy synchrotron radiation, studies using more conventional equipment require significantly greater concentrations (14). Nevertheless, these techniques have provided surprisingly consistent information regarding the structural organization of CLDCs that has been shown to agree with statistical thermodynamic models (29).

* This work was supported by Valentis, Inc. The costs of publication of this article were defrayed in part by the payment of page charges. This article must therefore be hereby marked "*advertisement*" in accordance with 18 U.S.C. Section 1734 solely to indicate this fact.

§ Supported by the American Foundation for Pharmaceutical Education. Present address: Dept. of Immunology (IMM-19), The Scripps Research Institute, 10550 N. Torrey Pines Rd., La Jolla, CA 92037.

¶ Present address: Molecular Biophysics & Biochemistry Dept., Yale University, 260 Whitney Ave., P.O. Box 208114, New Haven, CT 06520-8114.

** To whom correspondence should be addressed: Dept. of Pharmaceutical Chemistry, University of Kansas, 2095 Constant Ave., Lawrence, KS 66047. E-mail: middaugh@ku.edu.

[1] The abbreviations used are: CLDC, cationic lipid-DNA complex; cryo-EM, cryoelectron microscopy; SAXS, small angle x-ray scattering; FRET, fluorescence resonance energy transfer; DOTAP, 1,2-dioleoyl-3-trimethylammonium-propane; DDAB, dimethyldioctadecylammonium bromide; DOPE, 1,2-dioleoyl-*sn*-glycero-3-phosphoethanolamine; DOPC, 1,2-dioleoyl-*sn*-glycero-3-phosphocholine; HOC, Hoechst 33258; BODIPY-PE, 2-(4,4-difluoro-5,7-diphenyl-4-bora-3a,4a-diaza-*s*-indacene-3-pentanoyl)-1-hexadecanoyl-*sn*-glycero-3-phosphoethanolamine; BODIPY-PC, 2-(4,4-difluoro-5-(4-phenyl-1,3-butadienyl)-4-bora-3a,4a-diaza-*s*-indacene-3-pentanoyl)-1-hexadecanoyl-*sn*-glycero-3-phosphocholine.

Another technique that can potentially provide detailed information about the spatial organization of cationic lipids and DNA in CLDCs is fluorescence resonance energy transfer (FRET). Relationships describing the nonradiative transfer of energy from a donor fluorophore to a two-dimensional array of acceptor fluorophores embedded in a lipid bilayer have been derived (30–32). These relationships have been used to determine the distance of closest approach of proteins to membrane surfaces (33–37). We have used this approach to describe the association of DNA with cationic lipids as a function of charge ratio as well as membrane composition. The effect of ionic strength on the association of DNA with cationic bilayers has also been explored. Correlations with measurements of the distance of closest approach of DNA to the cationic lipid bilayer and the colloidal size of the complexes are also reported.

EXPERIMENTAL PROCEDURES

Materials—Supercoiled plasmid DNA (pMB290, >95% supercoiled) was obtained from Valentis Inc. The lipids 1,2-dioleoyl-3-trimethylammonium-propane (DOTAP), dimethyldioctadecylammonium bromide (DDAB), 1,2-dioleoyl-*sn*-glycero-3-phosphoethanolamine (DOPE) and 1,2-dioleoyl-*sn*-glycero-3-phosphocholine (DOPC) were obtained from Avanti Polar Lipids (Alabaster, AL). The fluorescent dyes Hoechst 33258 (HOC), 2-(4,4-difluoro-5,7-diphenyl-4-bora-3a,4a-diaza-*s*-indacene-3-pentanoyl)-1-hexadecanoyl-*sn*-glycero-3-phosphoethanolamine (BODIPY-PE), and 2-(4,4-difluoro-5-(4-phenyl-1,3-butadienyl)-4-bora-3a,4a-diaza-*s*-indacene-3-pentanoyl)-1-hexadecanoyl-*sn*-glycero-3-phosphocholine (BODIPY-PC) were obtained from Molecular Probes (Eugene, OR). The Cy3 LabelIT™ kit was obtained from Panvera (Madison, WI). All of the other chemicals were from Fisher.

Preparation of Cationic Lipid-DNA Complexes—Liposomes were first prepared by placing the required amount of a chloroform solution containing cationic lipid as well as DOPE or DOPC and various amounts of fluorescently labeled lipids in a glass vial and evaporating the solvent under a stream of nitrogen gas. The resulting lipid film was then placed under vacuum for a minimum of 2 h before hydrating in the appropriate Tris buffer with vortexing. After equilibrating at room temperature for 30 min, the liposomes were extruded 11 times through a 100-nm pore polycarbonate membrane. The liposomes were stored at 4 °C and typically used within 3 days. For fluorescence studies, DNA was first labeled either noncovalently with HOC at a 1:150 dye/bp ratio or covalently with Cy3 using the manufacturer's instructions at a 1:50 dye:bp ratio. CLDCs were formed by mixing various amounts of DNA with an equal volume of a cationic liposome solution with stirring for 20 s. The final cationic lipid concentration was 80 μM to maintain DOTAP above its reported critical micelle concentration of 70 μM (38). The complexes were allowed to equilibrate for 20 min before performing measurements. All of the charge ratios are indicated as positive:negative in the text.

Fluorescence Spectroscopic Measurements—Fluorescence spectra of CLDCs labeled with either HOC (excitation/emission, 358/462 nm) and BODIPY-PE (536/558 nm) or Cy3 (550/578 nm) and BODIPY-PC (586/597 nm) were obtained at 25 °C with a Quantamaster™ spectrofluorometer equipped with a 75-watt xenon lamp (PTI, Monmouth, NJ) using an excitation and emission bandwidth of 3 nm. A quartz cuvette (1 cm (ex) × 0.2 cm (em)) was used for all studies. For studies with HOC, a 370-nm-long pass filter was used between the sample and the photomultiplier tube. The quantum yield of HOC-labeled CLDCs was determined using quinine sulfate in 0.1 N H_2SO_4 as a reference (Q = 0.7), whereas that of Cy3-labeled CLDCs was determined using tetramethylrhodamine in methanol as a reference (Q = 0.68) using Equation 1.

$$Q_D = Q_R = \frac{I_D}{I_R}\frac{OD_R}{OD_D}\frac{n_D^2}{n_R^2} \quad \text{(Eq. 1)}$$

Here, Q is the quantum yield, I is the integrated intensity from 400 to 600 nm in the case of HOC and 560 to 620 nm for Cy3, OD is the optical density at the excitation wavelength, and n is the refractive index of the solution. The D subscript refers to the donor fluorophore, and the R subscript indicates the reference fluorophore of known quantum yield.

Correction for light scattering was made by subtracting the signal produced by the unlabeled sample. Corrections for the inner filter effect were performed using the following equation based on the Beer-Lambert Law.

$$I_{corr} = I(e^{(OD_{ex}l_{ex})} + e^{(OD_{em}l_{em})}) \quad \text{(Eq. 2)}$$

Where OD_{ex} and OD_{em} are the optical densities at the donor excitation and emission wavelengths, and l_{ex} and l_{em} are half the pathlengths for the excitation and emission axes, respectively.

Calculation of the Forster Distance for Donor Acceptor Pairs—The Förster distance (R_0) for each donor acceptor pair, which represents the distance of half-maximal transfer efficiency, was determined using the following equation.

$$R_0^6 = 8.79 \times 10^{-25}[\kappa^2 n^{-4} Q_D J(\lambda)] \quad \text{(Eq. 3)}$$

Where, κ^2 is the orientation factor between donor and acceptor molecules, n is the refractive index of the medium between donor and acceptor, Q_D is the quantum yield of the donor, and $J(\lambda)$ is the overlap integral of donor emission and acceptor absorption spectra (in units of M^{-1} cm^{-1} nm^4) given by the following equation.

$$J(\lambda) = \frac{\int_0^\infty F_D(\lambda)\varepsilon_A(\lambda)\lambda^4 d\lambda}{\int_0^\infty F_D(\lambda) d\lambda} \quad \text{(Eq. 4)}$$

$F_D(\lambda)$ and $\epsilon_A(\lambda)$ are the donor emission and acceptor extinction at a given wavelength, λ, respectively.

Determination of the Distance of Closest Approach for Donor-labeled DNA and BODIPY-labeled Cationic Lipids—Assuming that the approach of a DNA-bound donor fluorophore to the acceptor labeled lipid bilayer can be modeled as a point donor and an infinite plane of randomly distributed acceptors, the distance of closest approach, L, can be obtained from plots of I_{DA}/I_D *versus* the surface density, σ, of the acceptor molecules in the lipid bilayer, where I_{DA} and I_D are the fluorescence intensities of the donor in the presence or absence of acceptor, respectively. It has been previously shown that these two values are related by the following equation (30).

$$\frac{I_{DA}}{I_D} = 1 + \frac{\pi\sigma R_0^2}{2}\left(\frac{R_0}{L_{app}}\right)^4 \quad \text{(Eq. 5)}$$

where L_{app} is the apparent distance of closest approach and R_0 is described in Equation 3. The density of acceptor in the bilayer is determined using the following relation.

$$\sigma = 2\frac{[A]}{a[CL]_T} \quad \text{(Eq. 6)}$$

where [A] is the acceptor concentration, $[CL]_T$ is the total lipid concentration in the cationic liposomes, and a is the average cross-sectional area of the lipid headgroups. The latter is assumed to be 70 Å for DOTAP (14), (70 + 65)/2 = 67.5 Å for DOTAP:DOPE (39), (70 + 80)/2 = 75 Å for DOTAP:DOPC (39), and 60 Å for DDAB (40). The value of 2 on the right side of the equation reflects the fact that the DNA is presumably sandwiched between two bilayers, effectively doubling the acceptor concentration. Equation 6 is essentially equivalent to the Stern-Volmer relationship describing fluorescence quenching, with σ representing the two-dimensional concentration of quencher. It has been previously demonstrated that when $R_0/L < 0.6$, $L = L_{app}$ (30, 31, 35). In the case where $R_0/L_{app} > 0.6$, a correction must be made that takes the following form.

$$L = L_{app}\gamma^{1/4} \quad \text{(Eq. 7)}$$

where the correction factor, γ, is interpolated from data presented in Table I of Yguerabide (30). Further verification of L can be obtained by comparison of donor quenching with biexponential approximations to theoretical curves derived by Wolber and Hudson (31).

Dynamic Light Scattering—The samples were prepared in Tris buffer, pH 7.4, containing either no or 150 mM NaCl that had been filtered through 0.2-μm polysulfone filters (Gelman Science). All of the glassware was exhaustively washed with distilled and deionized water that had been similarly filtered. The measurements were taken using a light scattering instrument (Brookhaven Instruments Corp., Holtszille, NY) employing a 50 mW HeNe diode laser (λ = ~532 nm). The scattered light was monitored 90° to the incident beam, and the autocorrelation function was generated by a digital correlator (BI-9000AT). The data were collected continuously for five 20-s intervals for each sample and averaged. The autocorrelation function was fit by the method of cumulants to yield the mean diffusion coefficient of the complexes. The data

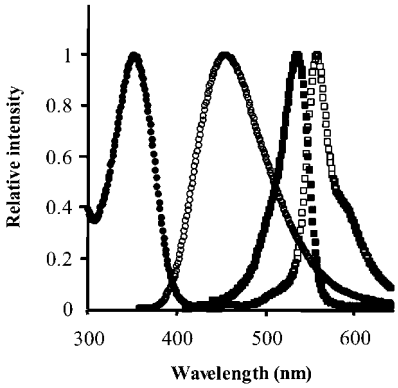

FIG. 1. **Fluorescence excitation (*solid symbols*) and emission (*open symbols*) spectra of HOC (*circles*) and BODIPY-PE (*squares*).**

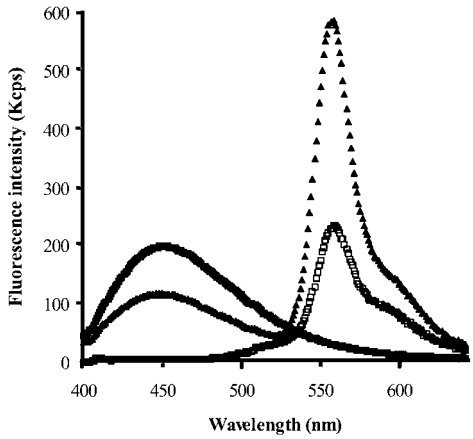

FIG. 2. **Fluorescence emission spectra of 3:1 +/− DOTAP:DNA labeled with HOC at a ratio of 1 dye (150 bp, *solid squares*), BODIPY-PE at a ratio of 1 dye (300 lipids, *open squares*) and both HOC and BODIPY-PE (*triangles*).** The DOTAP concentration was 80 μM.

are reported for a quadratic fit. The effective hydrodynamic diameter was obtained from the diffusion coefficient by the Stokes-Einstein equation.

RESULTS

To determine the distance of closest approach between DNA and the cationic lipid bilayer in CLDCs using FRET, DNA was labeled with the minor groove binding dye, HOC, and the lipid bilayer with a BODIPY-labeled lipid. It has been previously shown that HOC remains bound in the DNA minor groove when the DNA is condensed with cationic lipids.[2] The lipid label BODIPY-PE was chosen for several reasons. First, its spectral properties, *e.g.* large and environmentally insensitive extinction coefficient (41) and excellent spectral overlap with the HOC donor, make it applicable for a variety of lipid systems. Second, it is located in the apolar region of the lipid bilayer (41), which makes its mobility less sensitive to binding of DNA as shown previously for other dyes located in the apolar and interfacial regions of the bilayer (42).

Determination of the Forster Distance—The excitation and emission spectra of HOC and BODIPY-PE are shown in Fig. 1. The quantum yield as well as the wavelength of the emission maximum of HOC in CLDCs has been previously shown to depend on the type of lipid present as well as the charge ratio.[2] An increase in Q_D and a blue shift in the wavelength of emission maximum are generally observed upon binding to lipids. Thus, R_0 was calculated for each CLDC using individual values of Q_D and $J(\lambda)$. Surprisingly, R_0 was found to be 39 ± 1 Å for all CLDCs examined, presumably because of the compensating effects of increased quantum yields and decreased areas of spectral overlap (Equation 3). Calculations of R_0 were made assuming a random distribution of orientations between donor and acceptor ($\kappa^2 = 2/3$). The refractive index was taken to be 1.4 (35, 37), and Q_D and $J(\lambda)$ fell between 0.38 and 0.50 and 7.7×10^{14} and 9.5×10^{14} M^{-1} cm^{-1} nm^4, respectively.

FRET Studies with CLDCs—Binding of HOC-DNA to BODIPY-labeled cationic lipids results in a decrease in the fluorescence intensity of HOC and sensitized emission of the BODIPY probe (Fig. 2). For CLDCs composed of DOTAP and DNA, plots of I_{DA}/I_D *versus* the density of BODIPY on the bilayer (σ) demonstrate a linear dependence of HOC fluorescence intensity on the density of BODIPY-PE in the cationic bilayer as predicted from Equation 5 (Fig. 3*A*). The slope of the line increases as the ratio of DOTAP to DNA is increased, indicating a closer association of DNA with the lipid bilayer at higher charge ratios. Similar results are obtained when DNA is complexed with DOTAP:DOPE, DOTAP:DOPC, and DDAB (Fig. 3, *B*, *C*, and *D*, respectively). Energy transfer was essentially completely inhibited upon the addition of a 50-fold molar excess of the polyanion heparin, which has been previously demonstrated to cause the release DNA from these complexes (Ref. 43 and data not shown). The apparent distance of closest approach, L_{app}, was calculated from the slope of the lines using Equation 5 and corrected as previously described using Equation 7 (30) to obtain the mean distance of closest approach, L. These data are summarized in Fig. 4*A*. At a charge ratio of 0.5:1, the average distance between DNA and the probe in DOTAP bilayers is 45 ± 2 Å (*black bars*). This distance decreases as the charge ratio is increased to between 19 and 21 Å at ratios > 2:1. When the charge density of DOTAP bilayers is reduced by incorporating equimolar amounts of DOPE or DOPC, similar trends in the distance of closest approach as a function of CLDC charge ratio are observed (Fig. 4*A*, *white* and *stippled bars*, respectively). Comparison with a second cationic lipid (DDAB) again demonstrates a similar trend in the distance of closest approach (Fig. 4*A*, *striped bars*). The distance of closest approach appears to be significantly greater in DDAB compared with DOTAP CLDCs, however. For DDAB CLDCs below charge neutrality the distance is 52 ± 3 Å, whereas those above charge neutrality possess a distance of 24 ± 2 Å.

The effect of ionic strength on the distance of closest approach was examined for DOTAP CLDCs. When prepared in the presence of 150 mM NaCl, linear plots of I_{DA}/I_D *versus* σ are still observed (Fig. 3*E*), and a similar dependence of the slope on the on the charge ratio of the complex is still present (Fig. 4*B*). For DOTAP CLDCs prepared below a charge ratio of 3:1 +/−, increasing the ionic strength significantly increases the distance of closest approach by as much as 9 Å (Fig. 4*B*). At charge ratios above 3:1 +/−, the distance is not affected by the increased ionic strength.

To verify the measured distances between cationic lipid and DNA using the approach of Yguerabide (30), we compared the quenching of HOC fluorescence by BODIPY acceptors with a series of biexponential approximations to theoretical quenching curves for various ratios of L to R_0 (31). The approximations for various values of L are shown as *solid lines* in Fig. 5 and agree with theoretical values to within 1%. Although the absolute values of L cannot be obtained from the experimental curves, it can be estimated that 0.5:1 DOTAP CLDCs possess a distance of closest approach slightly less than 47 Å (Fig. 5, *diamonds*), whereas the distance separating HOC-DNA and

[2] C. M. Wiethoff, M. L. Gill, G. S. Koe, J. G. Koe, and C. R. Middaugh (2002) *J. Pharm. Sci.*, in press.

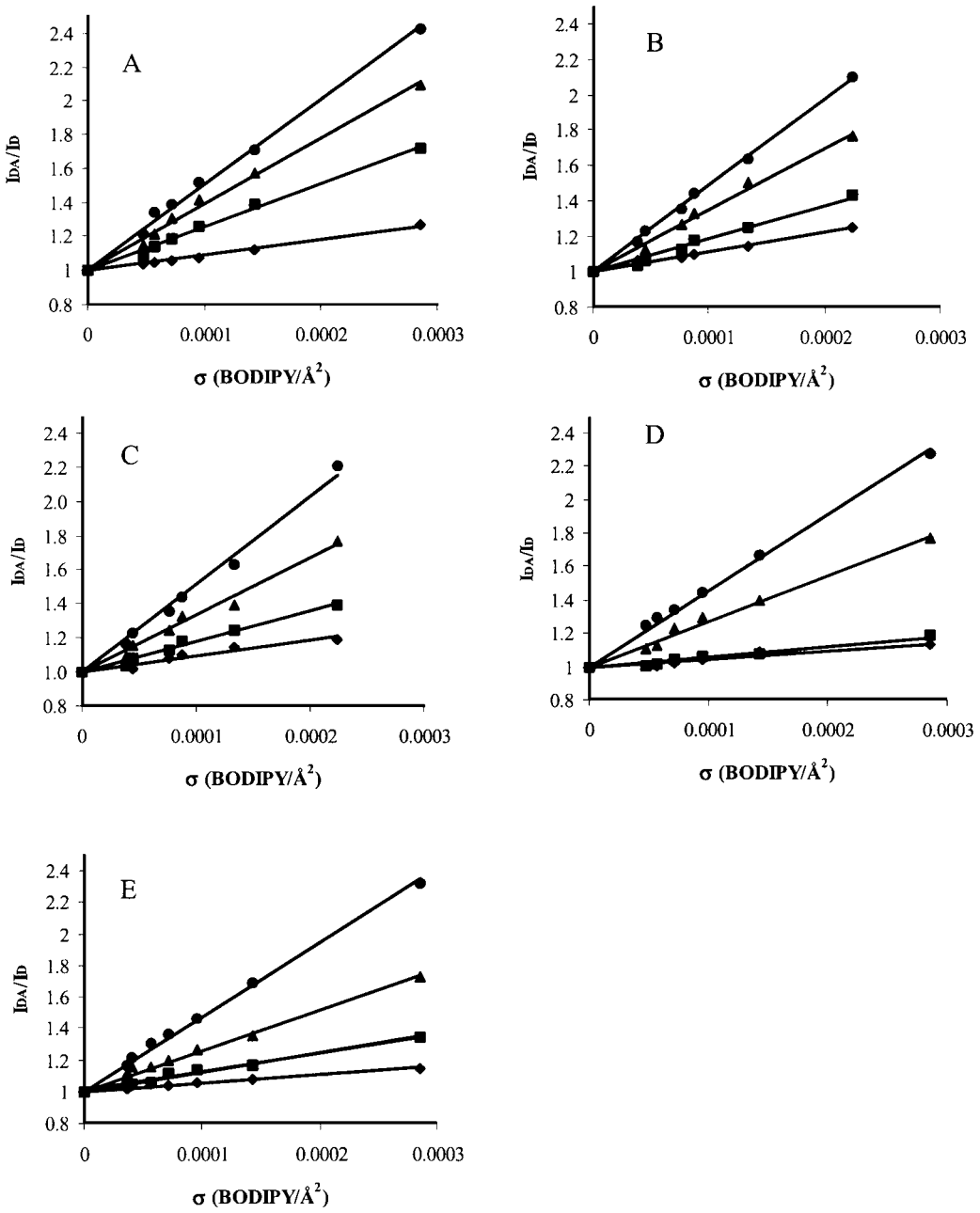

FIG. 3. **Representative quenching profiles for HOC-DNA in CLDCs containing increasing amounts of BODIPY-PE at charge ratios of 0:5:1 +/− (*diamonds*), 1:1 (*squares*), 2:1 (*triangles*), and 3:1 (*circles*).** *A*, DOTAP CLDCs. *B*, DOTAP:DOPE CLDCs. *C*, DOTAP:DOPC CLDCs. *D*, DDAB CLDCs. *E*, DOTAP CLDCs with 150 mM NaCl. *Solid lines* represent linear fits to Equation 5. The data for 4:1 and 5:1 ± CLDCs are not shown because they typically overlap with the data for 3:1 +/− CLDCs.

the BODIPY label in DOTAP bilayers is between 35 and 31 Å for 1:1 complexes (Fig. 5, *squares*). Positively charged 2:1 DOTAP CLDCs produce a value of L corresponding to just under 27 Å, whereas 3:1 complexes produce a value close to 20 Å. These distances are in excellent agreement with values obtained using Equation 5 (compare with Fig. 4).

To further confirm the accuracy of this approach, a Cy3-BODIPY-PC FRET donor-acceptor pair was used to measure the distance of closest approach. In this case, the Cy3 donor was covalently attached to the DNA. The excitation and emission spectra of Cy3 and BODIPY-PC are shown in Fig. 6. The quantum yield of Cy3 is 0.03, and the area of spectral overlap, $J(\lambda)$, is 3.5×10^{15} M^{-1} cm^{-1} nm^4. Assuming κ^2 to be 2/3 and the refractive index to be 1.4, R_0 is calculated to be 31 ± 1 Å. As seen with the HOC-BODIPY-PE pair, Cy3 fluorescence is decreased as the density of BODIPY-PC is increased in the DOTAP bilayer (Fig. 7). For calculation of the distance of closest approach for this FRET pair using Equations 5 and 7 above, we obtain a value of 21 ± 2 Å. This is in very good agreement with the value of 19 ± 1 Å obtained using the HOC-BODIPY-PE pair (Fig. 4).

Determination of the Mean Hydrodynamic Size of CLDCs—The mean diameter of the CLDCs was determined by dynamic light scattering as a function of charge ratio and lipid composition (Fig. 8). For DOTAP CLDCs with or without DOPE or DOPC, the size gradually increases as the charge ratio is increased from 0.5:1 to 1:1, with 0.5:1 DOTAP CLDCs having a mean diameter of 150 nm (*black bars*). Incorporating equimolar amounts of DOPE or DOPC into CLDCs results in mean diameters that are 10–20% greater than DOTAP alone for complexes below 1:1 (Fig. 8*A*, *white* and *stippled bars*, respectively). Complexes become colloidally unstable between charges ratio

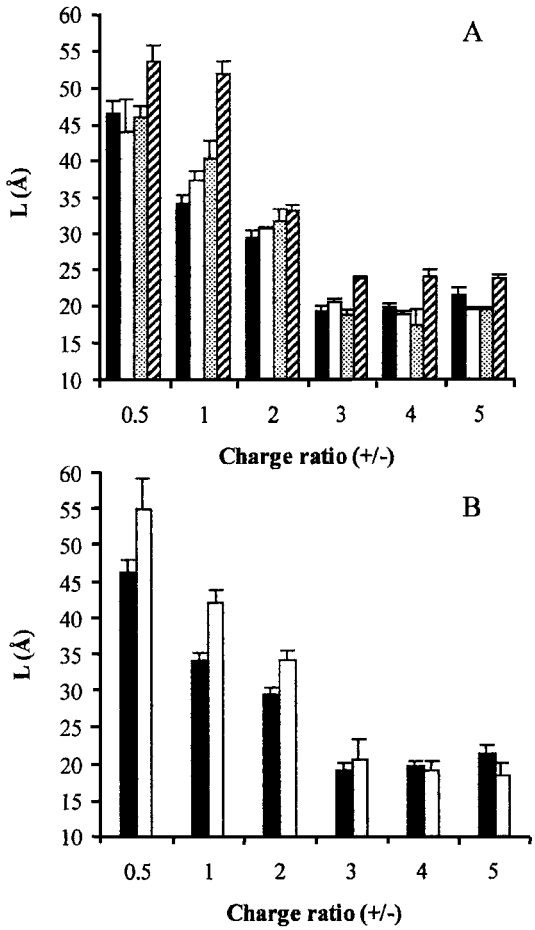

FIG. 4. **Calculated values of the distance of closest approach of HOC-DNA to BODIPY-PE in CLDCs as a function of charge ratio.** The values were calculated from data in Fig. 3 using Equations 5 and 7. The data represent the averages and standard errors for at least three replicates. *A*, DOTAP (*solid bars*), DOTAP:DOPE (*open bars*), DOTAP:DOPC (*stippled bars*), and DDAB (*striped bars*). *B*, DOTAP, 10 mM Tris (*solid bars*), and DOTAP, 10 mM Tris, 150 mM NaCl (*open bars*).

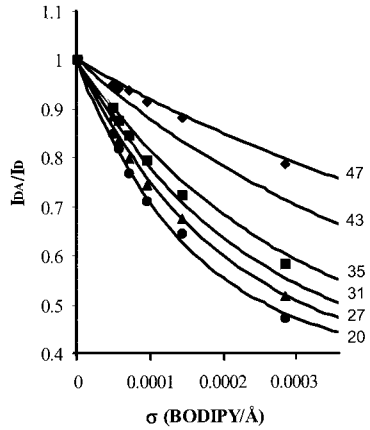

FIG. 5. **Comparison of HOC quenching to biexponential approximations of theoretical curves for energy transfer in two dimensions derived by Wolber and Hudson (31).** The *solid lines* represent theoretical curves for various values of L in Å as indicated to the *right* of the graph. The data points represent typical HOC quenching in DOTAP CLDCs at various charge ratios. 0:5:1 +/− (*diamonds*), 1:1 (*squares*), 2:1 (*triangles*), and 3:1 (*circles*).

of 1:1 and 2:1 because of charge neutralization (13). Above charge neutrality, DOTAP containing CLDCs show a maximal size at 2:1, with incorporation of equimolar amounts of DOPE

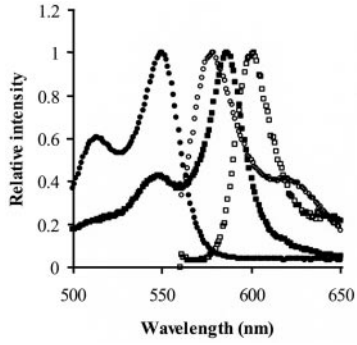

FIG. 6. **Fluorescence excitation (*solid symbols*) and emission (*open symbols*) spectra of Cy3 (*circles*) and BODIPY-PC (*squares*).**

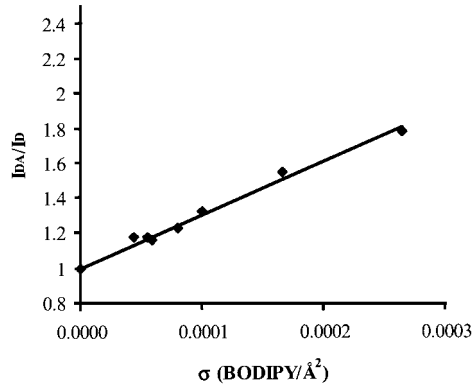

FIG. 7. **Representative quenching profile of Cy3-DNA in 3:1 +/− DOTAP CLDCs.** The *solid line* represents the linear fit to Equation 5.

or DOPC having little effect on particle size. The mean size of DDAB CLDCs is 30–40% greater than DOTAP CLDCs when prepared below charge neutrality (Fig. 8*A*, *striped bars*). For positively charged CLDCs, DDAB complexes are four to five times larger than DOTAP CLDCs. Upon increasing the ionic strength with 150 mM NaCl, DOTAP CLDCs display a 40–50% increase in the hydrodynamic size for complexes prepared at charge ratios of 2:1 and below (Fig. 8*B*). In the presence of 150 mM NaCl, charge neutrality in the complexes occurs between charge ratios of 2 and 3:1 (13). Complexes prepared above 3:1 are four to five times greater in size at the higher ionic strength.

DISCUSSION

Fluorescence resonance energy transfer has been used extensively to estimate the proximity of a variety of proteins to lipid membranes using the approach described above (33–37). This study represents an initial attempt to use this technique to obtain high resolution details about the association of cationic lipids with DNA. Using FRET, distances between DNA bound donor fluorophore and acceptor embedded in the apolar regions of the lipid bilayer were found to be reproducible with standard errors in the estimates typically less than 5% of the mean. Systematic errors arising from uncertainty in Q_D, $J(\lambda)$, and κ^2, however, may influence absolute values of the observed distances. These errors would be expected to effect each system studied similarly. Thus, comparisons between different CLDCs should still be valid. In determining Q_D and $J(\lambda)$, the error was less than 3%. The greatest degree of uncertainty arises from the inability to measure κ^2. It is typical to assume a value of 2/3, which assumes a random orientation between the donor and acceptor fluorophores. In general, the error introduced by assuming κ^2 to be 2/3 is ~10% when donor-acceptor pairs

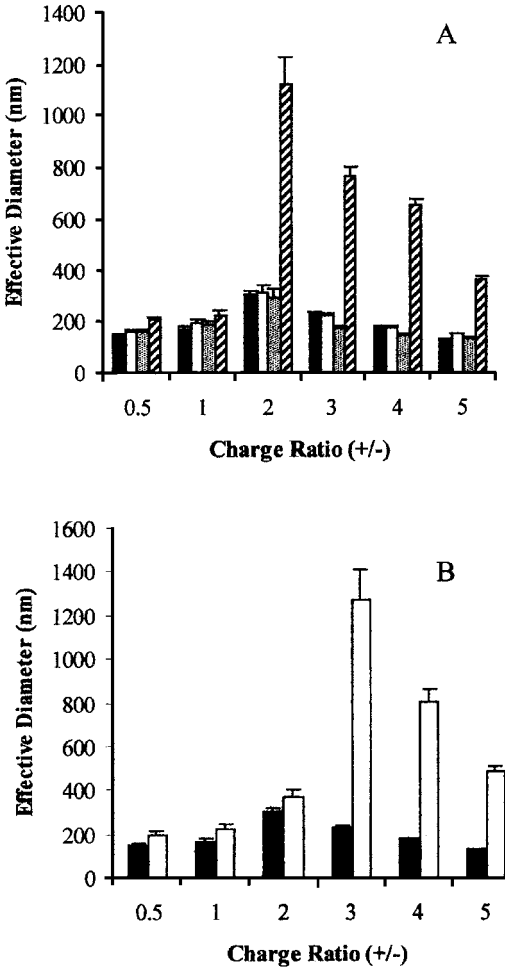

FIG. 8. **Hydrodynamic size of CLDCs determined by DLS.** The data represent the means and standard errors of three separate measurements. *A*, DOTAP (*solid bars*), DOTAP:DOPE (*open bars*), DOTAP:DOPC (*stippled bars*), and DDAB (*striped bars*). *B*, DOTAP, 10 mM Tris (*solid bars*) and DOTAP, 10 mM Tris, 150 mM NaCl (*open bars*).

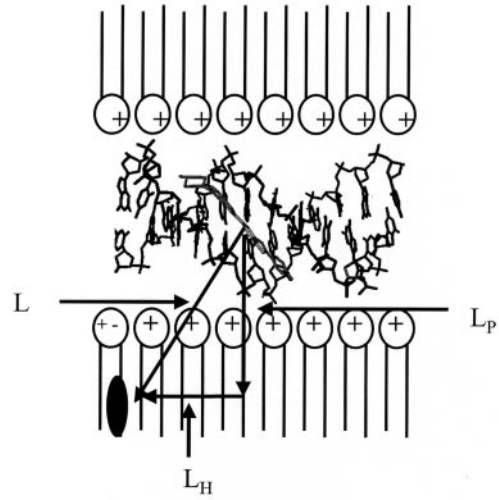

FIG. 9. **Model to estimate the distance of closest approach of HOC to the lipid bilayer as described under "Discussion."**

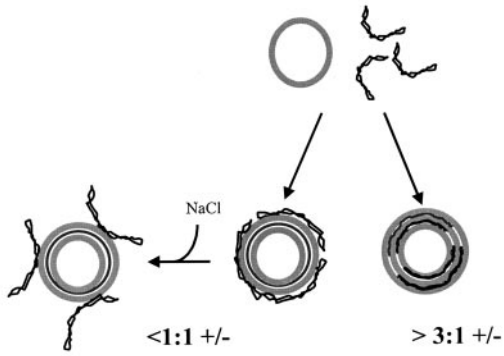

FIG. 10. **Proposed models for the structural arrangement of CLDCs prepared at different charge ratios or in the presence of increased ionic strength as described under "Discussion."**

possess anisotropy values less than 0.3 (44). This has been shown to be the case for BODIPY in several bilayers of differing fluidity (41) and HOC bound to DNA (45).

To facilitate interpretation of the physical meaning of the observed distances between HOC-DNA and the BODIPY-labeled lipid, the theoretical distance of closest approach was estimated based on the model in Fig. 9. In the model, L, the distance of closest approach, is related to the distance between the planes of HOC and BODIPY (L_p), and the horizontal distance between the dyes is transposed onto the same plane (L_H) by the following simple Pythagorean geometric relationship,

$$L^2 = L_p^2 + L_H^2 \qquad \text{(Eq. 8)}$$

For studies of the distance of a particular group on a protein from the lipid bilayer, the values of L_H have been necessary for calculations of L because the protein is often embedded in the lipid bilayer resulting in exclusion of the lipid dye from regions directly beneath the donor. In the case of CLDCs, the DNA can be assumed to not significantly penetrate the bilayer. Recent evidence from molecular dynamics simulations suggests that lipids with zwitterionic headgroups can, in fact, interact directly with the negatively charged DNA phosphates (46) suggesting that L_H is effectively 0. Therefore L represents the vertical distance between the donor and acceptor fluorophores.

In this model, HOC is assumed to be regularly distributed around the circumference of the DNA double helix. Hence, its distance from the bilayer surface would be the average of distances, which is taken to be 12.5 Å, or the radius of B-form DNA (47). This distance would also be applicable to Cy3-labeled DNA. The BODIPY probe is expected to be buried in the apolar region of the bilayer. Because BODIPY is much more hydrophobic than other commonly used probes such as NBD, its location in the bilayer is thought to correlate well with the length of the alkyl chain connecting it to the lipid headgroup (41). Assuming a thickness of ~4 Å for the interfacial region of the lipid, 0.95 Å/methylene group of the alkyl chain and a length of the BODIPY along its long axis of 9 Å, the average distance of BODIPY from the bilayer surface would be ~12 Å (3 + (5 × 0.95) + 9/2). Thus, we can estimate the closest distance between HOC and BODIPY to be ~25.5 Å.

For DOTAP CLDCs prepared at or above a 3:1 charge ratio in which the entire DNA is presumably entrapped in multilamellar structures between the lipid bilayers, the observed distance of closest approach is around 20 Å. The difference between the observed and calculated distances is slightly greater than the uncertainty introduced by the assumed value for κ^2. Alternatively, the distance may be expected to decrease based on the significant amount of bound water displaced from the lipid-DNA interface upon interaction (17, 48). The radius of B-form DNA in condensed phases has been estimated to be closer to 10 Å, which would bring our estimate of the closest possible distance to 23 Å. The remaining discrepancy could be accounted for by displacement of bound water from the lipid interface.

When DOTAP CLDCs are prepared below 3:1 ratios, the

distance between DNA and lipid becomes significantly greater than 20 Å, manifesting a maximal distance around 45 Å for 0.5:1 complexes. Xu *et al.* (6) have previously shown by density gradient centrifugation that two distinct types of CLDCs are formed, depending on the ratio of cationic lipid to DNA when they are mixed. For complexes formed by mixing lipid and DNA at ratios greater than 3:1, the actual ratio of cationic lipid to DNA phosphate in the complex saturates at ~3:1 +/−. Likewise, for CLDCs formed by mixing lipid and DNA at ratios below 0.5:1, the actual ratio of cationic lipid complexed to DNA in the particles is typically found to be 0.5:1 even at the lower charge ratios. In each case the complexes exist in the presence of unassociated lipid or DNA, respectively. Because we are measuring average values of L, it seems most probable that measured values of L in complexes formed between charge ratios of 0.5 and 3:1 represent the weighted average of L for these two types of complexes. Proposed models for these two complexes are shown in Fig. 10. For the negatively charged CLDCs, the observed distance of ~45 Å would arise from the average distance of closely associated DNA within the multilamellar particles and more loosely associated DNA molecules at the particle surface. Because the localization of DNA in these negatively charged CLDCs is more heterogeneous, with DNA presumably entrapped between lipid bilayers and at the particles surface, a greater degree of uncertainty is present in the measured distance of closest approach of DNA to the bilayer. This is due to the method used to calculate the two-dimensional density of the BODIPY acceptor molecules in the membrane based on the model presented in Fig. 9. Nevertheless, this model is supported by previous observations of the accessibility of DNA in the CLDCs to nucleases (28, 49–51) and intercalating dyes (21, 49, 52, 53) as well as the fact that complexes prepared at these charge ratios possess a negatively charged surface as assessed by measuring the zeta potential of the particle (13, 17, 19, 28). Additionally, cryo-EM of negatively charged complexes have described particles possessing what are presumably DNA "spikes" protruding from their surface similar to the model proposed in Fig. 10 (6). Positively charged CLDCs contain completely charge-neutralized DNA, which is maximally associated with cationic bilayers. In these CLDCs, the DNA is completely protected from nucleases and intercalating dyes and possesses a net positive zeta potential, suggesting that the exterior of the particles is composed primarily of cationic lipids. These studies also agree with SAXS results that describe lamellar repeat distances equivalent to the thickness of the lipid bilayer and a single DNA double helix (10, 25). Because SAXS studies rely on correlations within ordered repeating structures, however, they do not readily describe the extended DNA structures on the surface of the negatively charged CLDCs proposed in Fig. 10 and observed by cryo-EM (6).

Incorporation of DOPE or DOPC into positively charged DOTAP CLDCs results in similar values for the distance between DNA and the lipid bilayer ranging from 18 to 21 Å, suggesting little effect of bilayer charge density on the proximity of the DNA strands to the lipid. This is in contrast to the effect membrane charge density has on the interhelical spacing of DNA as observed by SAXS (10). Perhaps more interesting is the fact that DOTAP:DOPE CLDCs show similar trends in L compared with DOTAP CLDCs. Complexes of DOTAP:DOPE with linear λ-phage DNA have previously been shown to coexist as inverted hexagonal and lamellar structures (15). In an inverted hexagonal structure, a cylindrical distribution of acceptor molecules around the DNA double helix would negate the averaging in the distance of HOC from the lipid surface, resulting in a significant decrease in this distance from 12.5 Å to effectively 0. Thus, a distance of closest approach of HOC to BODIPY would be expected to be closer to ~12 Å. Because a marked decrease in L is not observed for DOTAP:DOPE CLDCs compared with DOTAP alone, the existence of nonlamellar phases is not apparent.

Studies with DDAB demonstrate a marked increase in the average distance of DNA from the bilayer. For negatively charged CLDCs, this distance is 7–17 Å greater than observed for DOTAP. For positively charged CLDCs, the value of L is 4 Å greater than that observed for DOTAP. In negatively charged CLDCs, the increased distance probably reflects the differences in the association of DNA on the particle surface (Fig. 10). Closer interhelical spacing of DNA because of the slight increase in charge density for DDAB compared with DOTAP (*e.g.* 1 charge/60 and 70 $Å^2$, respectively) may further extend the unbound portion of DNA away from the surface. Alternatively, for positively charged complexes, it has been shown that DDAB does not cause the same degree of dehydration of DNA as DOTAP (17).

Increasing the ionic strength more dramatically perturbs the average distance between DNA and lipid in complexes prepared below charge neutrality. For negatively charged CLDCs, the increased average distance between DNA and lipid presumably results from the decreased association of DNA with the surface of the particle or extension of unbound regions of DNA away from the particle (Fig. 10). The reason for the lack of effect of ionic strength on the distance between DNA and lipid in positively charged CLDCs is unclear. The differential effect of increased ionic strength on positively and negatively charged CLDCs correlates with observed effects on DNA interhelical spacing observed using SAXS where the spacing increased slightly for negatively charged CLDCs but remained unchanged for positively charged complexes (14).

Correlations between the distance of DNA from the cationic bilayer and the hydrodynamic size of the complexes are mixed. For negatively charged complexes, it appears that the increased distance observed by FRET coincides with an increase in the hydrodynamic size of CLDCs containing only cationic lipids. This agrees with the model presented in Fig. 10 in which changes in L reflect changes in the association of DNA with the surface of the particles. In the case of positively charged CLDCs, no correlation between L and the hydrodynamic size is apparent. The much larger size of DDAB CLDCs in this charge regime probably reflects aggregation of complexes caused by the destabilization of the rigid DDAB bilayer. Reductions in particle size by fluidizing the DDAB bilayer upon incorporation of DOPE or cholesterol have been previously reported (17). For DOTAP CLDCs at higher ionic strength, the much larger size observed may also result from aggregation in this case caused by the reduced electrostatic repulsion between particles.

In conclusion, we have demonstrated the utility of FRET to define structural features of CLDCs representing a variety of compositions. These studies support the multi-lamellar model of CLDCs observed by SAXS and cryo-EM. Most significantly, this approach permits the examination of these nonviral gene delivery complexes in the solution state and at concentrations nearer physiologically relevant values using equipment commonly available in most laboratories.

REFERENCES

1. Chadwick, S. L., Kingston, H. D., Stern, M., Cook, R. M., O'Connor, B. J., Lukasson, M., Balfour, R. P., Rosenberg, M., Cheng, S. H., Smith, A. E., Meeker, D. P., Geddes, D. M., and Alton, E. W. (1997) *Gene Ther.* **4,** 937–942
2. Waddill, W., III, Wright, W., Jr., Unger, E., Stopeck, A., Akporiaye, E., Harris, D., Grogan, T., Schluter, S., Hersh, E., and Stahl, S. (1997) *AJR Am. J. Roentgenol.* **169,** 63–67
3. McLachlan, G., Ho, L. P., Davidson-Smith, H., Samways, J., Davidson, H., Stevenson, B. J., Carothers, A. D., Alton, E. W., Middleton, P. G., Smith, S. N., Kallmeyer, G., Michaelis, U., Seeber, S., Naujoks, K., Greening, A. P., Innes, J. A., Dorin, J. R., and Porteous, D. J. (1996) *Gene Ther.* **3,** 1113–1123
4. Nishikawa, M., and Huang, L. (2001) *Hum. Gene Ther.* **12,** 861–870

5. Zuidam, N. J., Hirsch-Lerner, D., Margulies, S., and Barenholz, Y. (1999) *Biochim. Biophys. Acta* **1419,** 207–220
6. Xu, Y., Hui, S. W., Frederik, P., and Szoka, F. C., Jr. (1999) *Biophys. J.* **77,** 341–353
7. Tarahovsky, Y. S., Rakhmanova, V. A., Epand, R. M., and MacDonald, R. C. (2002) *Biophys. J.* **82,** 264–273
8. Smisterova, J., Wagenaar, A., Stuart, M. C., Polushkin, E., ten Brinke, G., Hulst, R., Engberts, J. B., and Hoekstra, D. (2001) *J. Biol. Chem.* **276,** 47615–47622
9. Simberg, D., Danino, D., Talmon, Y., Minsky, A., Ferrari, M. E., Wheeler, C. J., and Barenholz, Y. (2001) *J. Biol. Chem.* **276,** 47453–47459
10. Radler, J. O., Koltover, I., Salditt, T., and Safinya, C. R. (1997) *Science* **275,** 810–814
11. MacDonald, R. C., Ashley, G. W., Shida, M. M., Rakhmanova, V. A., Tarahovsky, Y. S., Pantazatos, D. P., Kennedy, M. T., Pozharski, E. V., Baker, K. A., Jones, R. D., Rosenzweig, H. S., Choi, K. L., Qiu, R., and McIntosh, T. J. (1999) *Biophys. J.* **77,** 2612–2629
12. Lobo, B. A., Rogers, S. A., Choosakoonkriang, S., Smith, J. G., Koe, G., and Middaugh, C. R. (2002) *J. Pharm. Sci.* **91,** 454–466
13. Lobo, B. A., Davis, A., Koe, G., Smith, J. G., and Middaugh, C. R. (2001) *Arch. Biochem. Biophys.* **386,** 95–105
14. Koltover, I., Salditt, T., and Safinya, C. R. (1999) *Biophys. J.* **77,** 915–924
15. Koltover, I., Salditt, T., Radler, J. O., and Safinya, C. R. (1998) *Science* **281,** 78–81
16. Kennedy, M. T., Pozharski, E. V., Rakhmanova, V. A., and MacDonald, R. C. (2000) *Biophys. J.* **78,** 1620–1633
17. Choosakoonkriang, S., Wiethoff, C. M., Anchordoquy, T. J., Koe, G. S., Smith, J. G., and Middaugh, C. R. (2001) *J. Biol. Chem.* **276,** 8037–8043
18. Solodin, I., Brown, C. S., Bruno, M. S., Chow, C. Y., Jang, E. H., Debs, R. J., and Heath, T. D. (1995) *Biochemistry* **34,** 13537–13544
19. Eastman, S. J., Siegel, C., Tousignant, J., Smith, A. E., Cheng, S. H., and Scheule, R. K. (1997) *Biochim. Biophys. Acta* **1325,** 41–62
20. Mok, K. W., and Cullis, P. R. (1997) *Biophys. J.* **73,** 2534–2545
21. Gershon, H., Ghirlando, R., Guttman, S. B., and Minsky, A. (1993) *Biochemistry* **32,** 7143–7151
22. Huebner, S., Battersby, B. J., Grimm, R., and Cevc, G. (1999) *Biophys. J.* **76,** 3158–3166
23. Battersby, B. J., Grimm, R., Huebner, S., and Cevc, G. (1998) *Biochim. Biophys. Acta* **1372,** 379–383
24. Schmutz, M., Durand, D., Debin, A., Palvadeau, Y., Etienne, A., and Thierry, A. R. (1999) *Proc. Natl. Acad. Sci. U. S. A.* **96,** 12293–12298
25. Lasic, D. D., Strey, H., Stuart, M. C. A., Podgornik, R., and Frederik, P. M. (1997) *J. Am. Chem. Soc.* **119,** 832–833
26. Farhood, H., Serbina, N., and Huang, L. (1995) *Biochim. Biophys. Acta* **1235,** 289–295
27. Song, Y. K., Liu, F., Chu, S., and Liu, D. (1997) *Hum. Gene Ther.* **8,** 1585–1594
28. Birchall, J. C., Kellaway, I. W., and Mills, S. N. (1999) *Int. J. Pharm.* **183,** 195–207
29. Harries, D., May, S., Gelbart, W. M., and Ben-Shaul, A. (1998) *Biophys. J.* **75,** 159–173
30. Yguerabide, J. (1994) *Biophys. J.* **66,** 683–693
31. Wolber, P. K., and Hudson, B. S. (1979) *Biophys. J.* **28,** 197–210
32. Dewey, T. G., and Hammes, G. G. (1980) *Biophys. J.* **32,** 1023–1035
33. Baird, B., Shopes, R. J., Oi, V. T., Erickson, J., Kane, P., and Holowka, D. (1989) *Int. Arch. Allergy Appl. Immunol.* **88,** 23–28
34. Baird, B., and Holowka, D. (1985) *Biochemistry* **24,** 6252–6259
35. Shahrokh, Z., Verkman, A. S., and Shohet, S. B. (1991) *J. Biol. Chem.* **266,** 12082–12089
36. Shaklai, N., Yguerabide, J., and Ranney, H. M. (1977) *Biochemistry* **16,** 5585–5592
37. Fernando Valenzuela, C., Weign, P., Yguerabide, J., and Johnson, D. A. (1994) *Biophys. J.* **66,** 674–682
38. Zuidam, N. J., and Barenholz, Y. (1997) *Biochim. Biophys. Acta* **1329,** 211–222
39. Marsh, D. (ed) (1990) *CRC Handbook of Lipid Bilayers*, CRC Press, Boca Raton, FL
40. Okuyama, K., Soboi, Y., Iijima, N., Hirabayashi, K., Kunitake, T., and Kijayama, T. (1988) *Bull. Chem. Soc. Jpn.* **61,** 1485–1490
41. Johnson, I. D., Kang, H. C., and Haugland, R. P. (1991) *Anal. Biochem.* **198,** 228–237
42. Hirsch-Lerner, D., and Barenholz, Y. (1998) *Biochim. Biophys. Acta* **1370,** 17–30
43. Wiethoff, C. M., Smith, J. G., Koe, G. S., and Middaugh, C. R. (2001) *J. Biol. Chem.* **276,** 32806–32813
44. Haas, E., Katchalski-Katzir, E., and Steinberg, I. Z. (1978) *Biochemistry* **17,** 5064–5070
45. Araki, T., Yamamoto, A., and Yamada, M. (1987) *Histochemistry* **87,** 331–338
46. Bandyopadhyay, S., Tarek, M., and Klein, M. L. (1999) *J. Phys. Chem. B* **103,** 10075–10080
47. Podgornik, R., Rau, D. C., and Parsegian, V. A. (1994) *Biophys. J.* **66,** 962–971
48. Hirsch-Lerner, D., and Barenholz, Y. (1999) *Biochim. Biophys. Acta* **1461,** 47–57
49. Bhattacharya, S., and Mandal, S. S. (1998) *Biochemistry* **37,** 7764–7777
50. Crook, K., McLachlan, G., Stevenson, B. J., and Porteous, D. J. (1996) *Gene Ther.* **3,** 834–839
51. Ferrari, M. E., Nguyen, C. M., Zelphati, O., Tsai, Y., and Felgner, P. L. (1998) *Hum. Gene Ther.* **9,** 341–351
52. Crook, K., Stevenson, B. J., Dubouchet, M., and Porteous, D. J. (1998) *Gene Ther.* **5,** 137–143
53. Even-Chen, S., and Barenholz, Y. (2000) *Biochim. Biophys. Acta* **1509,** 176–188

LIPIDS AND LIPOPROTEINS:

The Structural Organization of Cationic Lipid-DNA Complexes

Christopher M. Wiethoff, Michelle L. Gill, Gary S. Koe, Janet G. Koe and C. Russell Middaugh

J. Biol. Chem. 2002, 277:44980-44987.
doi: 10.1074/jbc.M207758200 originally published online September 23, 2002